Key Points:
- Stable isotopes in tropical water vapor are evaluated in modern and future high-CO_2 simulations using water isotope-enabled GCMs
- Midtropospheric isotope ratios capture dynamical processes related to the strength of the Walker circulation in a warming atmosphere
- The West-East Pacific gradient in isotope ratios provides a fingerprint of circulation changes, a target for future satellite retrievals

Supporting Information:
- Supporting Information S1

Correspondence to:
S. G. Dee,
sylvia@ig.utexas.edu

Tracking the Strength of the Walker Circulation With Stable Isotopes in Water Vapor

Sylvia G. Dee[1,2,3] [ID], **Jesse Nusbaumer**[4] [ID], **Adriana Bailey**[5,6] [ID], **James M. Russell**[1,2], **Jung-Eun Lee**[1,2] [ID], **Bronwen Konecky**[7], **Nikolaus H. Buenning**[8], and **David C. Noone**[9] [ID]

[1]Department of Earth, Environmental, and Planetary Sciences, Brown University, Providence, RI, USA, [2]Institute at Brown for Environment and Society, Brown University, Providence, RI, USA, [3]Institute for Geophysics, University of Texas, Austin, Austin, TX, USA, [4]NASA Goddard Institute for Space Studies, New York, NY, USA, [5]Department of Earth Sciences, Dartmouth College, Hanover, NH, USA, [6]National Center for Atmospheric Research, Boulder, CO, USA, [7]Department of Earth and Planetary Sciences, Washington University, St. Louis, MO, USA, [8]Department of Earth Sciences, University of Southern California, Los Angeles, CA, USA, [9]College of Earth, Ocean, and Atmospheric Sciences, Oregon State University, Corvalis, OR, USA

Abstract General circulation models (GCMs) predict that the global hydrological cycle will change in response to anthropogenic warming. However, these predictions remain uncertain, in particular, for precipitation (Intergovernmental Panel on Climate Change, 2013, https://doi.org/10.1017/CBO9781107415324.004). Held and Soden (2006, https://doi.org/10.1175/JCLI3990.1) suggest that as lower tropospheric water vapor concentration increases in a warming climate, the atmospheric circulation and convective mass fluxes will weaken. Unfortunately, this process is difficult to constrain, as convective mass fluxes are poorly observed and incompletely simulated in GCMs. Here we demonstrate that stable hydrogen isotope ratios in tropical atmospheric water vapor can trace changes in temperature, atmospheric circulation, and convective mass flux in a warming world. We evaluate changes in temperature, the distribution of water vapor, vertical velocity (ω), advection, and water isotopes in vapor (δD_V). Using water isotope-enabled GCM experiments for modern versus high-CO_2 atmospheres, we identify spatial patterns of circulation change over the tropical Pacific. We find that slowing circulation in the tropical Pacific moistens the lower troposphere and weakens convective mass flux, both of which impact the δD of water vapor in the midtroposphere. Our findings constitute a critical demonstration of how water isotope ratios in the tropical Pacific respond to changes in radiative forcing and atmospheric warming. Moreover, as changes in δD_V can be observed by satellites, our results develop new metrics for the detection of global warming impacts to the hydrological cycle and, specifically, the strength of the Walker circulation.

1. Introduction

In recent decades, a large number of climate modeling studies have been devoted to constraining changes in the hydrological cycle that may occur with increased anthropogenic carbon dioxide emissions (e.g., Held & Soden, 2006; Huntington, 2006; Loaiciga et al., 1996; Seager et al., 2010; Wentz et al., 2007, and references therein), summarized in Intergovernmental Panel on Climate Change (2013). A robust feature in these simulations of global warming with general circulation models (GCMs) is an increase in atmospheric water vapor content. Water vapor is predicted to increase with temperature following Clausius-Clapeyron scaling (Jenkins, 2008), under which a 1 °C increase in temperature causes a 7% increase in total column water vapor. Despite the 7%/°C increase in specific humidity, global mean precipitation is predicted to increase by only 1.5–3% in the multimodel average (Held & Soden, 2006). This discrepancy is significant: the moisture balance of the atmosphere dictates that $P = M \cdot q$, where P is precipitation, M is convective mass flux, and q is specific humidity. Because the mean global precipitation rate must be balanced by moisture transport from the boundary layer to the free troposphere (M), vertical motion must decrease to maintain the surface energy and vapor budget (Betts, 1998; Held & Soden, 2006; Schneider et al., 2010; Soden & Held, 2006). The mass flux (M) in precipitating convective towers thus is predicted to decrease with increasing temperature (Vecchi et al., 2006), weakening mass exchange between the boundary layer and free troposphere (Vecchi et al., 2006).

In the tropical Pacific—a locus of convective transport for the global hydrological cycle—a decline in vertical mass flux between the boundary layer and free troposphere should weaken the Walker circulation. This reduction in the strength of the Walker circulation in response to climate warming is predicted by most GCMs (DiNezio et al., 2009; Vecchi et al., 2008, 2006), which suggest that the Walker circulation will weaken more than the zonally-symmetric Hadley circulation (Gastineau et al., 2009; Vecchi & Soden, 2007). However, there is still considerable debate about changes in the strength of vertical motion in the tropical Pacific, in part due to a paucity of instrumental observations prior to 1950 to test model predictions (e.g., Sandeep et al., 2014, and references therein). Indeed, in contrast to model predictions, satellite-derived, in situ, and proxy-based observations have reported a strengthening of the Walker circulation in recent decades (An et al., 2012; Carilli et al., 2014; Conroy et al., 2009; LHeureux et al., 2013; Sohn & Park, 2010; Tokinaga et al., 2012). While observations of sea level pressure (SLP) and sea surface temperature (SST) are commonly used to identify changes to the Walker cell, changes in the organization of the atmosphere and hydrological cycle in response to shifts in SLP and SST have proven difficult to detect; further, the dynamical mechanisms linking changes in SST and SLP with the mean circulation in the tropics may not be consistent in a warmer future mean state.

Part of the challenge understanding changes in the large-scale overturning circulation stems from the fact that vertical motion and vertical mass flux are not directly observable via satellite retrievals. Moreover, convective mass transport processes are not simulated explicitly in Intergovernmental Panel on Climate Change (IPCC)-class GCMs, and instead are parameterized and estimated at the subgrid scale. Identifying metrics that can trace the impact of anthropogenic warming on the tropical overturning circulation in observations and model simulations is therefore critical to detecting changes in the hydrological cycle.

To address this challenge, this study evaluates the ability of stable water isotopologues (HDO, $H_2^{18}O$) in tropospheric water vapor and precipitation to record changes in convective processes and mass fluxes associated with the Pacific Walker circulation. Because heavier isotopologues experience a lower saturation vapor pressure than their isotopically light counterparts, the isotope ratio of vapor (e.g., δD_V) can distinguish vapor masses with different condensation histories, including boundary layer versus free tropospheric air and convective mixing of the two (e.g., Bailey et al., 2015; Galewsky et al., 2016; Risi et al., 2012). We investigate hydrological changes and the isotopic responses to climate warming in the tropical Pacific using high-CO_2 simulations with isotope-enabled GCMs. We decompose these responses into a thermodynamic component, which depends solely on an increase in specific humidity due to warming (estimated using a single-column Rayleigh distillation model), and a dynamical component that we isolate by comparing the single-column distillation model to GCM simulations. Isolating this dynamic component allows us to evaluate isotopic changes driven by changes in the tropical overturning circulation.

This study documents substantial thermodynamic and dynamic impacts on δD_V that could be used to detect past, present, and future changes in the tropical hydrological cycle and, in particular, the strength of the Walker circulation. We demonstrate that water isotopes inform our interpretation of the atmospheric changes accompanying changes to the Walker cell in a way that SLP and SST changes alone cannot. We expect that moistening of the atmosphere accompanying warming should increase isotope ratios in the atmosphere; we find, in contrast to this prediction, that isotope ratios decrease in key regions of the Walker cell in response to dynamical changes alone. This yields a unique tracer for diagnosing future changes to the hydrological cycle in the tropical Pacific. Section 2 reviews the experimental design including GCM simulation details. Section 3 reviews our single-column, 1-D Rayleigh distillation model simulation and compares its prediction to water vapor isotope profiles from high-CO_2 atmosphere experiments in two state-of-the-art isotope enabled atmospheric GCMs. Finally, section 4 discusses the implications of our work for the validation of isotope-enabled GCMs, future remote sensing initiatives, paleoclimate data interpretation, and tracking changes in the Walker circulation.

2. Methods

We analyzed both modern and future high-CO_2 simulations from the isotope-enabled Community Atmosphere Model 5, iCAM5 (Nusbaumer et al., 2017) alongside predictions for both a modern and high-CO_2 atmosphere from a single-column Rayleigh distillation model. By design, the Rayleigh model calculates changes in isotope ratios caused by the change in humidity (q) that results from increasing temperature. We therefore expect isotopic changes predicted by this model to represent the isotopic response to thermodynamic perturbations. In contrast, the GCM calculates the full water isotopic response resulting from an array of

processes, including temperature, precipitation, humidity, circulation, and other dynamical changes. We compute the residuals of the predictions from the GCM simulations relative to the Rayleigh model to isolate the isotopic signature of changes in the tropical overturning circulation. In this manner, we differentiate changes in free tropospheric isotope ratios caused by thermodynamic factors, e.g. changes in temperature and specific humidity (ΔT, Δq), from those caused by dynamic factors (changes in moisture flux convergence, convective transport, and vertical velocity).

2.1. Idealized Single-Column Rayleigh Distillation Model

A single-column Rayleigh distillation model was initialized using temperature and pressure profiles taken from a tropical Pacific grid average in iCAM5, for both the modern control and the high-CO_2 future atmosphere (T_{mod}, T_{future}, p_{mod}, and p_{future}). We assume that the air parcel is saturated as the air is lofted vertically, and such that $q = q_s$ (specific humidity is equal to saturation specific humidity). Distillation was calculated for the same vertical resolution and lapse rate as iCAM5. Saturation vapor pressure (e_s) and the saturation specific humidity (q_s, g/kg) at each vertical level are then calculated via Clausius-Clapeyron scaling:

$$e_s = 610.78 \cdot \exp[(17.27 * T_{mod})/(T_{mod} + 237.3)] \tag{1}$$

$$q_s = \epsilon \cdot es/p_{mod} \tag{2}$$

where T is temperature in Celsius, p is pressure in hectopascal, and ϵ=0.622 (Wallace & Hobbs, 2006) for the future atmosphere and modern control. The single-column model estimates isotopic changes with height assuming a moist adiabatic lapse rate and Rayleigh distillation for stable isotopic fractionation (e.g., Sharp, 2007). The temperature-dependent equilibrium fractionation factor (α_{LIQ}) is calculated as follows:

$$\alpha = a_D/(T_{mod}^2) + b_D/T_{mod} + c_D \tag{3}$$

$$\alpha_{LIQ} = \exp(\alpha), \tag{4}$$

where $a_D = 24.844e + 3$, $b_D = -76.248$, and $c_D = 52.612e - 3$ (Majoube, 1971).

We imposed changes in temperature drawn from the GCM's future minus modern temperature profiles, using the mean tropical average profile for the Pacific [20°S to 20°N, 140°E to 270°E], to quantify the thermodynamically driven shift in the isotope profile. The value of δD is initialized to −80‰ at the surface, which is chosen as a characteristic mean value near the surface for vapor near equilibrium with sea water. The isotope ratio of vapor in each model layer changes following a Rayleigh relationship:

$$\delta D_V = (\delta D_V + 1{,}000) \cdot F^{(\alpha_{LIQ}-1)} - 1{,}000 \tag{5}$$

where δD is defined in units of per mille (and see section S1.1 in the supporting information for δ notation), F is the fraction of vapor remaining in each layer after distillation and is calculated as $F' = q'/q$, where F', q' are the fraction of vapor remaining and humidity in the k^{n+1} model layer, respectively, and F, q refer to the k^n model layer. In comparing these results to the GCM simulations to evaluate changes in mass flux (M), we focus on the degree to which water vapor isotope ratios in the region of the Walker cell deviate from the single-column Rayleigh distillation model, which serves as the null hypothesis.

In using the single-column model to estimate the thermodynamically-driven isotopic response, a key assumption is that the atmospheric lapse rate is closely approximated by a pseudoadiabat. This is representative of the moist humid tropics (Mapes, 2001; Park et al., 2014), but we acknowledge that changes in M could be different in the drier, unsaturated tropics, that is, outside of the current range of the Intertropical Convergence Zone (ITCZ). Thus, this assumption is likely more robust in the West Pacific than in the East Pacific. This must be considered when comparing differences between the GCM and single-column model in ascending and descending branches of the Walker circulation.

2.2. Isotope-Enabled GCM Experiments

We examined changes in T, q, vertical pressure velocity ω, δD_V, pressure (p), cloud water, advection, and evaporation minus precipitation (E−P) in isotope-enabled model simulations with two experiments: an RCP8.5 high-CO_2-forcing scenario (25 years), and a modern control (30 years). Three isotope-enabled models were initially investigated for this study (see supporting information for comparisons), but we here focus in detail
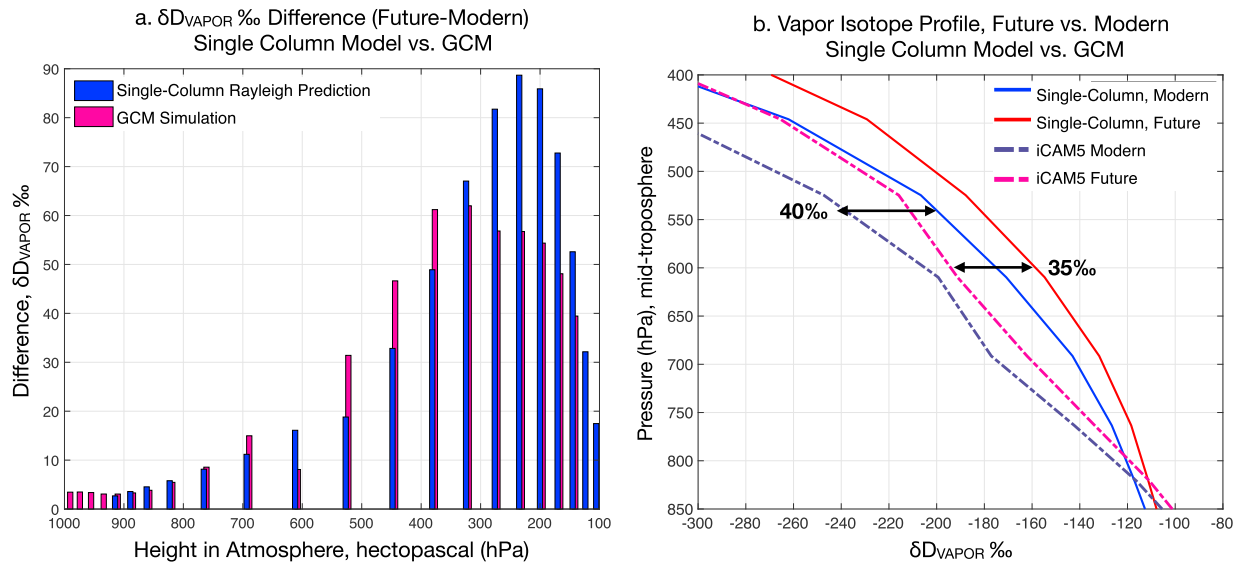
Figure 1. δD_V as a function of height in the atmosphere, single-column model versus GCM. Results for both high-CO_2 forcing (future) and control (modern) experiments, tropical Pacific domain, 20°S to 20°N. (a) Water vapor δD, future minus modern at each vertical level. (b) Vapor isotope profiles for single-column model (blue, red) versus iCAM5 (purple, pink), showing differences between single-column model prediction (Rayleigh-only) and full GCM (total isotopic response) simulation, with a focus on the midtroposphere. For (a), the Y axis indicates the difference in the δD_V between the experiment and the control; that is, more positive values mean that the experiment is more enriched in heavy HDO. The difference between the pink and blue bars in (a) represents the *non-Rayleigh* component of the response. GCM = general circulation model.

on results from iCAM5 (Nusbaumer et al., 2017), coupled to the isotope-enabled Community Land Model (Wong et al., 2017). For the iCAM5 simulations, modern SST/sea ice fields were taken from observations and averaged over the years 1974–1999 to produce an annual average climatology. For the high-CO_2 experiment, fields were taken from a bias-corrected fully coupled Community Earth System Model simulation with RCP8.5 forcing (Riahi et al., 2011) for the years 2074–2099 and were averaged to produce a new SST and sea ice field (Hurrell et al., 2013; Nusbaumer et al., 2017). The RCP8.5 forcing scenario is characterized by CO_2 concentrations approaching 1,000 ppm by the year 2100, and the forcing fields are described in detail in Riahi et al. (2011).

For completeness, we additionally evaluated a 4xCO_2 simulation with IsoGSM (Yoshimura et al., 2008) and a last millennium simulation of SPEEDY-IER (Dee, Noone, et al., 2015); we compare the *future* simulations of iCAM5 and IsoGSM in the supporting information in terms of temperature changes (Figure S2), circulation (Figures S3 and S4), isotope simulations (Figure S5), and advective tendencies for isotope ratios (Figures S9 and S10).

We calculated differences between the GCM and the single-column model predictions of δD_V for the future experiment minus the modern control at each vertical level to evaluate how the tropical overturning circulation impacts isotope ratios.

3. Results

3.1. Idealized Atmospheric Single-Column Experiment

In the idealized atmospheric column simulation of the warmer climate, the largest changes in δD_V between the experiment and the control occur in the upper troposphere, where isotope ratios are sensitive to large relative changes in T and q. Indeed, the Rayleigh model predicts an increase in δD_V of 20–30‰ in the midtroposphere (~500 hPa), and up to 90‰ in the upper troposphere (~200 hPa; see Figure 1a, blue bars indicate the change in the warming experiment minus the control). This suggests that a large portion, if not all, of the water isotope composition's response can result from thermodynamic changes in response to CO_2-induced warming (Figure 1a).

In comparison with the GCM simulation, large offsets between the pink and blue bars (showing warming minus modern changes in Figure 1a indicates the GCM simulates a larger change in δD_V at midelevations (~500-hPa level) than the single-column model, whereas the single-column model simulates larger changes
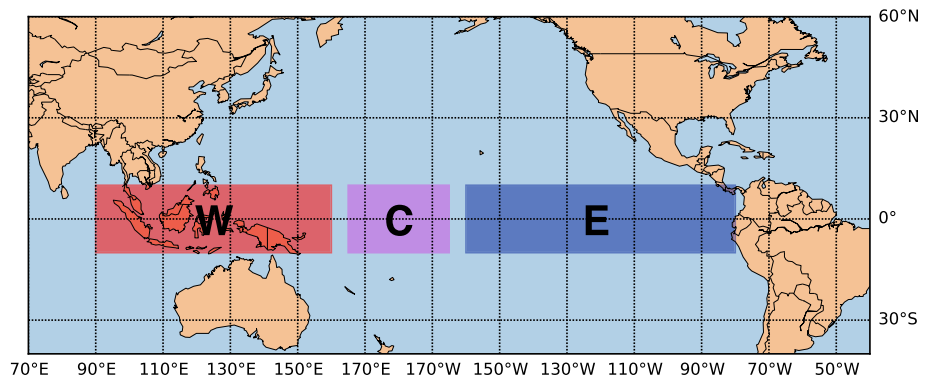
Figure 2. Defining regions of the Walker cell: For the purposes of this paper, we define the western, central, and eastern Pacific between 10°S and 10°N. Western (red shaded region) spans 90°E to 160°E. Central (purple shaded region) spans 165°E to 175°W. Eastern (blue shaded region) spans 160°W to 80°W. Adapted from definitions given in Vecchi et al. (2006) and Sandeep et al. (2014).

than the GCM at higher elevations (above ∼300 hPa). Further, water vapor δD_V profiles calculated with the GCM versus the single-column model are lower by 30–40‰, especially in the midtroposphere (Figure 1b). iCAM5 simulates lower δD_V (30–40‰) in the midtroposphere and is far less enriched in HDO than the single-column model in the upper troposphere. At higher altitudes, δD_V is more sensitive to large fractional changes in T, q, and thermodynamic effects dominate (both for the Rayleigh-only experiment and in the GCM). Finally, providing a q-specific reference frame, both simulations are plotted as a function of q and pressure in Figure S1. The q-δD_V diagram shows the Rayleigh-predicted response for the single-column model experiment versus the GCM. In the warmer atmosphere, Rayleigh curves shift toward higher humidity and more enriched δD_V.

The difference between the single-column model and the GCM can be explained by processes simulated in the GCM including convection and cloud physics, vertical and horizontal moisture transport (i.e., advection and convergence), and entrainment and detrainment (all relatonly response is essentiallyed to M), none of which are resolved by the Rayleigh model. Relative to the single-column model, the thermodynamic-only response is muted in the GCM, where water vapor mixing processes buffer the thermodynamic response. The differences indicate changes in circulation influence the water isotope ratios.

3.2. Atmospheric General Circulation Model Experiments

To analyze regional patterns of isotopic change in the GCM experiment, we first define the *western, central, and eastern* regions of the Walker cell (adapted from Sandeep et al., 2014; Vecchi et al., 2006). Figure 2 highlights these regions, and we refer to these definitions in the analyses that follow.

Temperature changes simulated by the GCM over the tropical Pacific are relatively zonally and vertically homogenous (Figure S1). With uniform warming of the atmosphere at all model levels, we expect a complimentary increase if δD_V is driven by thermodynamic/Rayleigh processes alone. Indeed, the response of δD_V to temperature is large and vertical changes in temperature and vapor are tightly coupled (e.g., Figures 1a and 1b). Simulated δD_V increases sharply in the troposphere as predicted by a purely thermodynamic response, highlighting the direct control of temperature on water isotopes in a warming climate. Temperature changes impact δD_V via temperature-dependent equilibrium fractionation (Majoube, 1971) and by increasing residual water vapor content in the atmosphere (F).

In the central tropical Pacific, however, there is considerably more horizontal and vertical structure in δD_V than in temperature, indicating changes in convection, mixing, and other processes that could result from a decelerating tropical circulation and reductions in the gross upward mass flux, M. Figures 3, S3, and S4 show the change in vertical velocity (ω) in the modern control, future warming experiment, and difference between them in the atmospheric GCM simulations. The variables M and ω are directly related via $M = w \cdot \rho$, $w = -\omega/(\rho \cdot g)$, where ρ is the atmospheric density and w is the vertical velocity in m/s (and see Schneider et al., 2010, for a more complete derivation). The two variables have been shown to scale similarly with climate change in an idealized GCM experiment (Schneider et al., 2010). Our use of M in this context refers to the time-mean, tropical gross upward mass flux, and does not explicitly account for transient convective circulations,
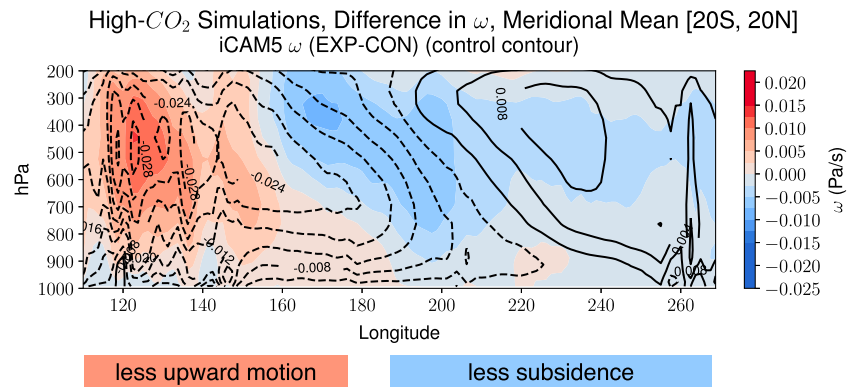
Figure 3. General circulation model changes in vertical velocity (ω) across the tropical Pacific. iCAM5 = 2xCO$_2$ experiment minus modern control, meridional mean (−20 to 20 latitude). Change in vertical velocity (ω) in the experiment minus the control in color filled contour plot. Black contour lines show control simulation. Sign convention is negative = upward motion, positive = downward motion. Thus, red colors in western Pacific indicate a reduction in the magnitude of the negative values in the control compared to the experiment, or less uplift. Blue colors indicate less positive values in the experiment compared to the control or less downward motion.

which are also substantial. Thus, the GCM simulation is consistent with a slowing of the Walker circulation: we observe less upward motion (convection) in the western/central tropical Pacific and less downward motion (subsidence) in the eastern tropical Pacific (Figure 3).

We expect an isotopic response to these processes in the midtroposphere, as δD_V is sensitive to changes in mixing and convection at these higher altitudes (Noone, 2012). By contrast, δD_V at the surface is affected by factors such as SSTs, surface wind speed, and surface humidity; the impacts of these surface processes are muted in the midtroposphere, and dynamical signals emerge. Deviating from the predicted thermodynamic response, midtropospheric isotope ratios *decrease* in certain regions in the high-CO$_2$ experiment (Figures 4b, 4c, S3, and S4). Some of the strongest changes in ω occur between 500 and 600 hPa, where we observe strong spatial coherency in the changes in ω and δD_V in the high-CO$_2$ atmosphere experiment and the modern control (Figures 4a and 4b). This result holds for altitudes between approximately 850 and 400 hPa. The simulations indicate decreasing subsidence in the central and eastern tropical Pacific coincide with enriched water isotope ratios, whereas less uplift in the western Pacific is spatially correlated with decreased δD_V.

To further investigate the relationship between atmospheric circulation changes and δD_V, we examined the changes in future minus modern δD_V at an altitude of 500–600 hPa in the tropical Pacific, as well as the meridional mean cross section of these fields at all altitudes (Figures 4, S3, and S4). We compared the GCM simulations to the prediction from the single atmospheric column model. This was achieved by modeling the predicted Rayleigh fractionation using the temperature profile for both the modern and high-CO$_2$ GCM experiments, which yields a temperature and moisture-driven δD_V response at every grid cell and at every pressure level, a value we term $\delta D_{\mathrm{RAYLEIGH}}$. Removing $\delta D_{\mathrm{RAYLEIGH}}$ from the actual modeled (δD_Z) isotope ratio at a given height for iCAM5 (defined here as $\delta D_{\mathrm{DYN}} = \delta D_Z - \delta D_{\mathrm{RAYLEIGH}}$, *DYN* for dynamic component) shows the predicted response of the water isotopes accompanying a deceleration of the Walker circulation (Figure 4c). Changes in δD_{DYN} (the residual) align with changes in ω in the midtroposphere.

3.3. Water Vapor Isotope Ratios as Tracers of Circulation Changes

As mentioned, water vapor isotope ratios are generally enriched in iCAM5's high-CO$_2$ future experiment; however, we observe several zones in the tropical Pacific where isotope ratios are, remarkably, more depleted in the high-CO$_2$ future simulations (Figure 4b). The simulated changes are consistent with satellite observations of δD_V climatology, specifically for El Niño versus La Niña events; during warmer months, observations indicate reduced isotope ratios in the western tropical Pacific in the midtroposphere (see Figure 9c). Values of δD_{DYN} further highlight these zones of depletion (Figure 4c); the future minus modern δD values are lower in the western Pacific (150–170°E) at 600 hPa. This is because δD_V is in part controlled by circulation changes: convective intensity directly affects the fraction of moisture detrained in the midtroposphere, and δD values in the troposphere are thus influenced by the height of convective detrainment. Convection in the midtroposphere tends to moisten the atmosphere and enrich δD through detrainment and sublimation of ice
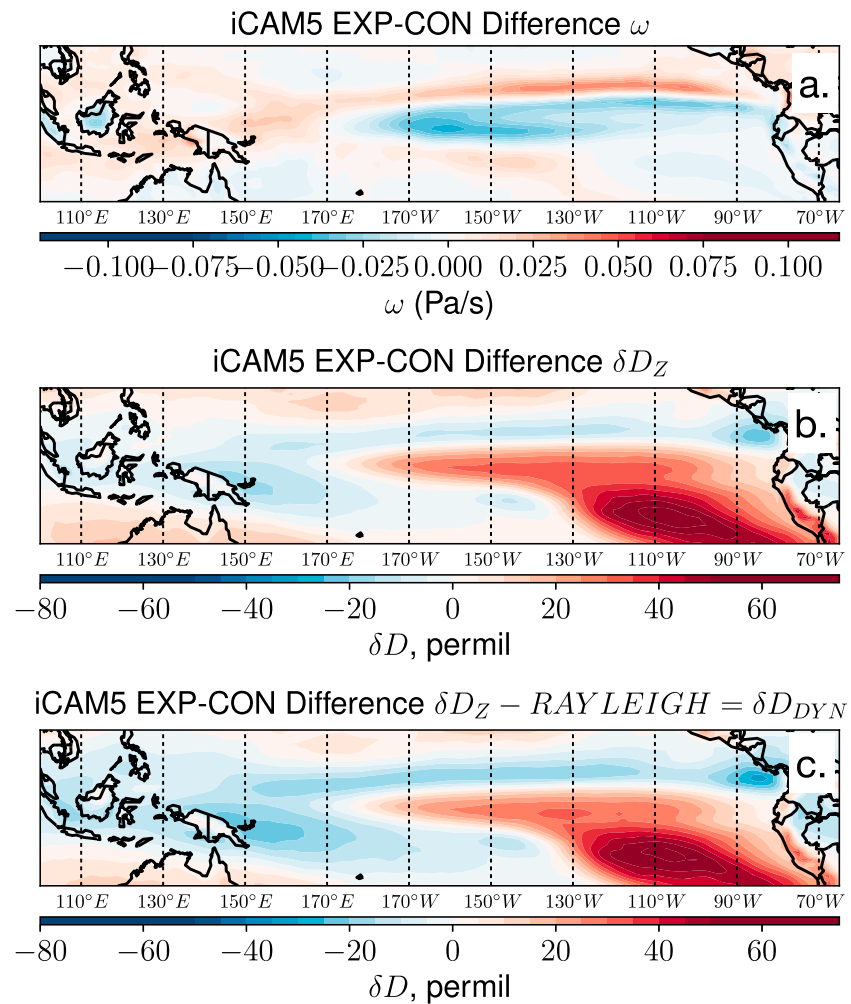
Figure 4. iCAM5 changes in circulation versus water isotope ratios in the midtroposphere (500–600 hPa). iCAM5 simulation: 2xCO$_2$ (2,100 A.D.) minus modern control. (a) Change in vertical velocity (ω). (b) Change in δD_V. (c) Change in simulated δD_V minus the Rayleigh-only component, yielding $\delta D_{Z-RAYLEIGH} = \delta D_{DYN}$. All fields were extracted for 500–600 hPa as a target atmospheric level for this study, as the largest negative changes in δD_V occur at this height.

crystals, both of which distribute water in higher levels of the atmosphere. By contrast, deep convection tends to deplete lower tropospheric water vapor via isotopically depleted downdrafts and rain reevaporation.

In the midtroposphere, the impacts of vertical motion and convection on δD are more difficult to constrain; isotopic tendencies depend jointly on advection, evaporation, condensation, and upper to lower tropospheric mixing effects, including the height of convective mixing and detrainment (Galewsky et al., 2016). We here explore each of these controls in succession via the examination of key moisture budget terms: ω, E−P, detrained moisture fraction, and advection.

3.3.1. Vertical Motion

Vertical motion (ω) is strongly tied to the isotopic composition of vapor in the midtroposphere (Figure 4). In the high-CO$_2$ experiments, we observe a decrease in δD_V in the midtroposphere over the western Pacific/Indo-Pacific Warm Pool (IPWP). This depletion is likely due to a decrease in upward motion (Figure 3) and convective mixing in the midtroposphere in the warmer atmosphere, consistent with a reduction in M. Conversely, δD_V increases in high-CO$_2$ simulations where the change in ω is negative (less subsidence), particularly in the midtroposphere (500 to 600 hPa; Figure 4, central/eastern Pacific). Decreasing subsidence allows for increased convection and enrichment in the midtroposphere in the central and eastern Pacific.
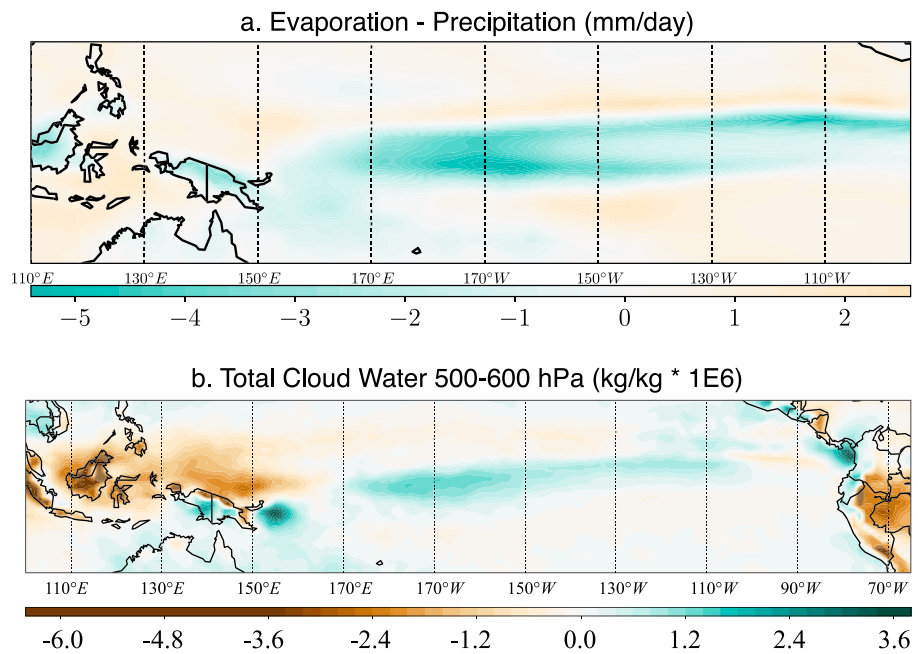
Figure 5. iCAM5: Changes in evaporation, precipitation, and cloud water. Future minus modern changes in the hydrological cycle, including (a) evaporation minus precipitation, future − modern, and (b) total change in cloud water at 500–600 hPa, future − modern.

Although deep convection detrains more boundary layer moisture into the midtroposphere, the δD of that moisture also depends heavily on conditions in the boundary layer. For example, detrained moisture in the western Pacific and along the ITCZ is often HDO-depleted due to a previous history of mixing and rain reevaporation (Noone, 2012). This necessitates investigation into the impacts of E−P, advection, and convergence on δD.

3.3.2. Evaporation Minus Precipitation

Previous studies suggest variations in δD_V independent of variations in humidity are sensitive to imbalances in E−P (Bailey et al., 2017; Lee et al., 2007). If water vapor moves upward, mixing in an atmospheric column without any precipitation, then, for a given moisture concentration, δD_V will be enriched compared to a column in which precipitation is occurring. Furthermore, in heavily precipitating regions, a net import of moisture is required to balance large differences in P and E, and this moisture convergence tends to further deplete the atmospheric column (assuming converged moisture has lost heavy isotopes through precipitation; Moore et al., 2014; Torri et al., 2017). In contrast, horizontal advection may cause δD_V to depart significantly from the change expected due to differences in E and P alone; advection of air masses sourced from remote regions will cause mixing, changing local isotope ratios. We thus expect that isotope ratios will most closely align with changes in E−P in places where changes in atmospheric convergence dominate the total hydrological change.

In the iCAM5 future simulation, E−P decreases in the central/equatorial Pacific (Figures 5a and S7) indicating higher precipitation, which should result in a local decrease in δD_V. However, δD_V increases (Figure 4c), which suggests advection from a non-local moisture source. It is possible that the increase in moisture advection is derived from the highly HDO-enriched air mass in the southeast Pacific. In this case, the advected δD_V in the midtroposphere may overwhelm the local E−P signal (which would act to deplete δD_V via increased rainout). In other words, in the central Pacific, the increase in δD_V is produced by the advection of enriched moisture from the southeast Pacific (described in detail below).

Dynamical impacts on δD_V are also apparent in the ITCZ and Warm Pool. We expect that where E−P increases (e.g., over the Indo-Pacific region), δD_V should also increase. Examining Figures 4c and 5a, δD_V in fact decreases in the midtroposphere, with a change as much as −20‰. This discrepancy requires contributions from a third source of HDO-depleted moisture via either horizontal advection or lofted cloud condensate. Given that E−P increases locally, the net moisture convergence should decrease. Further, the Warm Pool and ITCZ are net precipitating regions, which means that local vertical transport likely follows a Rayleigh line.
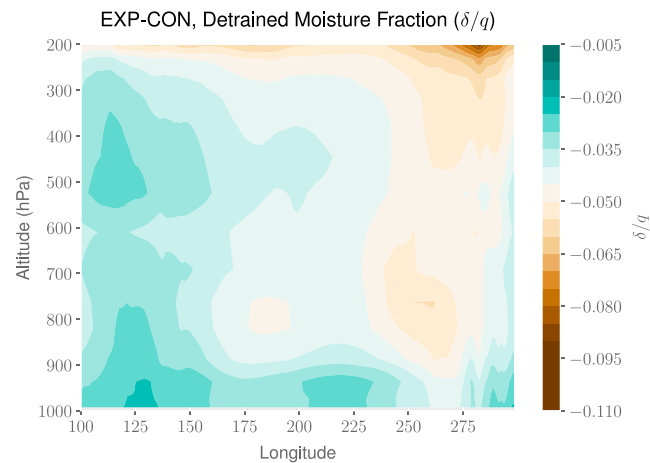
Figure 6. iCAM5 results: Detrained moisture fraction, δ/q, [10°S to 10°N], experiment minus control. Meridional average across the tropical Pacific for detrainment, showing the fractional change in detrained moisture with respect to the future − modern change in total moisture (q).

Less horizontal isotopic convergence shifts δD_V closer to the relatively depleted local Rayleigh values, and thus, the midtropospheric (500–600 hPa) water isotope ratios are lower in the high-CO_2 simulations.

3.3.3. Detrainment

Changes in vertical transport, including detrainment, also influence δD_V. iCAM5 includes a detrainment water tag which represents both locally and remotely-advected detrained moisture. Figures 5b and 6 indicate a modest reduction in cloud water and detrained moisture fraction in the Warm Pool region: convective clouds moisten the midtroposphere via detrainment, and the small decrease in detrained moisture at these altitudes may contribute to the decrease in δD_V. The relatively large decrease in the detrained moisture fraction, δ/q (Figure 6) in the East Pacific compared to the West Pacific results in a significant west-east gradient in the change in detrainment fraction (especially in the midtroposphere; see Figure S8). These changes align with changes in ω in the model, such that regions with less (more) subsidence experience a larger (smaller) decrease in detrained moisture fraction, linked to the strength of the tropical overturning circulation. Further, Figure 5b indicates changes in cloud water that confirm a reduction in water content reaching the 500- to 600-hPa level in the western Pacific, but an increase in total cloud water in the central and eastern regions, suggestive again of increased convection/reduced subsidence in the central Pacific but reduced upward motion in the west.

3.3.4. Advection

Finally, changes in advection in the high-CO_2 experiment impact isotope ratios in midtropospheric vapor. The advective tendencies for isotope ratios is given by

$$\frac{\delta R_i}{\delta t} = \vec{V} \cdot \nabla R_i, \qquad (6)$$

where R_i is the water isotope ratio HDO/H$_2^{16}$O, $\vec{V}$ is the 3-D wind field and ∇R_i is the centered difference of isotope ratios in every grid cell. Figure 7 shows the change in isotope ratios due to advection in the modern (a), future (b), and the future minus modern difference (c). In the control experiment (Figure 7a), the change in isotope ratios due to advection is positive in the central Pacific; positive isotope ratios in the central Pacific are advected west by prevailing easterlies. For reference, Figure 8 shows tropical Pacific wind vectors superposed on the isotope ratios in the midtroposphere. The easterlies weaken aloft in the future warming experiment (Figure 8), consistent with a weakening Walker cell. The reduced easterly strength corresponds to a reduction in the advection of isotopically enriched water vapor to the west, resulting in the lower advective tendencies between 170°E and 190°E in Figure 7c. Conversely, the advective tendencies support a modest increase (rather than the observed decrease) over the IPWP and Maritime Continent. In this region, the isotopic change is likely dominated by local vertical velocity changes.

In the eastern tropical Pacific, low isotope ratios above cold upwelling ocean waters (see Figure 8a) are advected toward the west in the modern, and this weakens in the future. The reduced advection of depleted
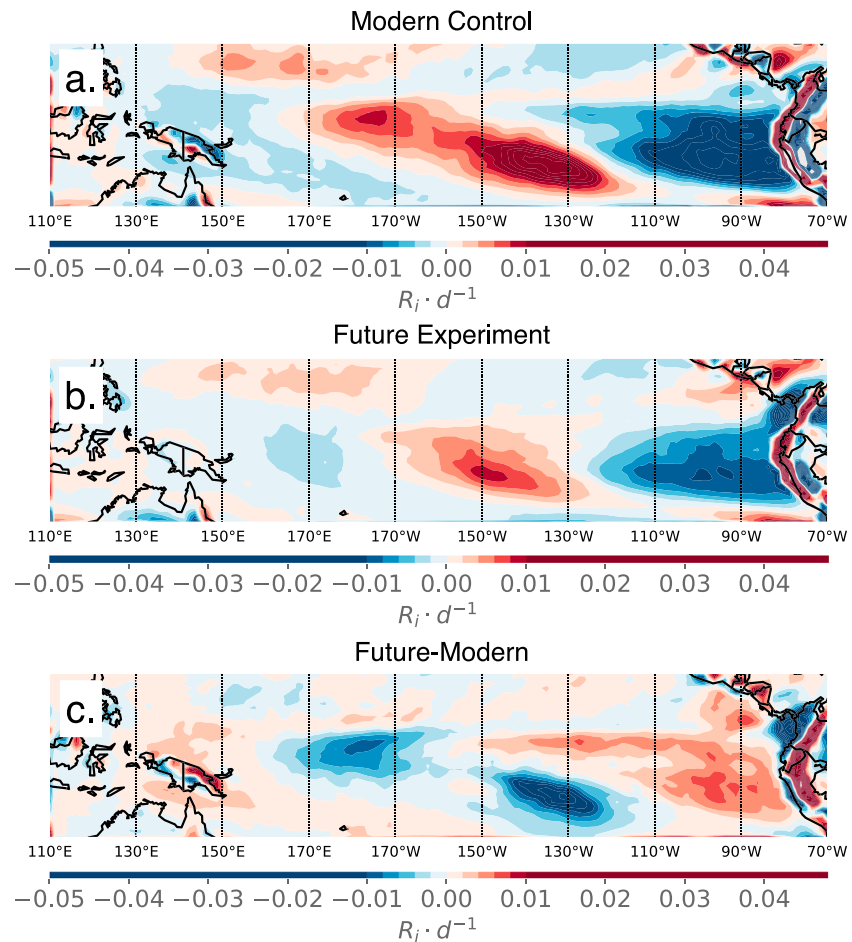
Figure 7. Advective tendencies for isotopes in water vapor, iCAM5. Change in water isotope ratios at 600 hPa due to advection, (a) control, (b) experiment, and (c) experiment minus control.

moisture drives isotope ratio tendencies higher in the eastern tropical Pacific, $\sim$130–90°W (Figure 7c). Thus, in the eastern Pacific, (1) isotope ratios increase due to temperature forcing in the warmer climate and (2) given less subsidence, higher isotope ratios, and slower easterlies, advection is positive. The advective tendencies for isotope ratios essentially respond to slower easterly winds in a warmer atmosphere (Figure 8c), and this contributes to reduced isotope ratios in the western and central tropical Pacific in the future experiment. Finally, the wind fields in Figure 8c suggest that there is additional transport of depleted IPWP moisture into the south central Pacific ($\sim$10°S, from 150°E to 150°W) via westerly wind anomalies in the experiment compared to the control, evident in the low isotopic advection tendencies in the same region shown in Figure 7c.

To summarize, with reduced easterlies and less subsidence in the east, high isotope ratios accumulate (rather than disperse, diverging outward due to subsidence, and advecting westward). We observe a coincident reduction in deep convection in the western and central Pacific, consistent with warming predictions. This convective change depletes the atmosphere in the western and central Pacific, allowing a depleted signal to be advected to the west Pacific $\sim$170°E. Finally, isotope ratios are highly sensitive to changes in the advection of moisture and are not controlled by changes in vertical velocity alone. Rather, the full signal indicates systematic reorganization of convection. This link suggests that changes in vertical velocity as they relate to water isotope ratios reflect, more broadly, the large-scale convective changes in the Walker cell.

Finally, we note that we do not show changes in convergence, as this term has a much smaller, if any, impact on isotope ratios. Convergence can increase or decrease moisture, but it also increases isotopic moisture at the same rate; thus, it does not produce a change in the actual ratio R. A derivation demonstrating this is given in section S1.3.
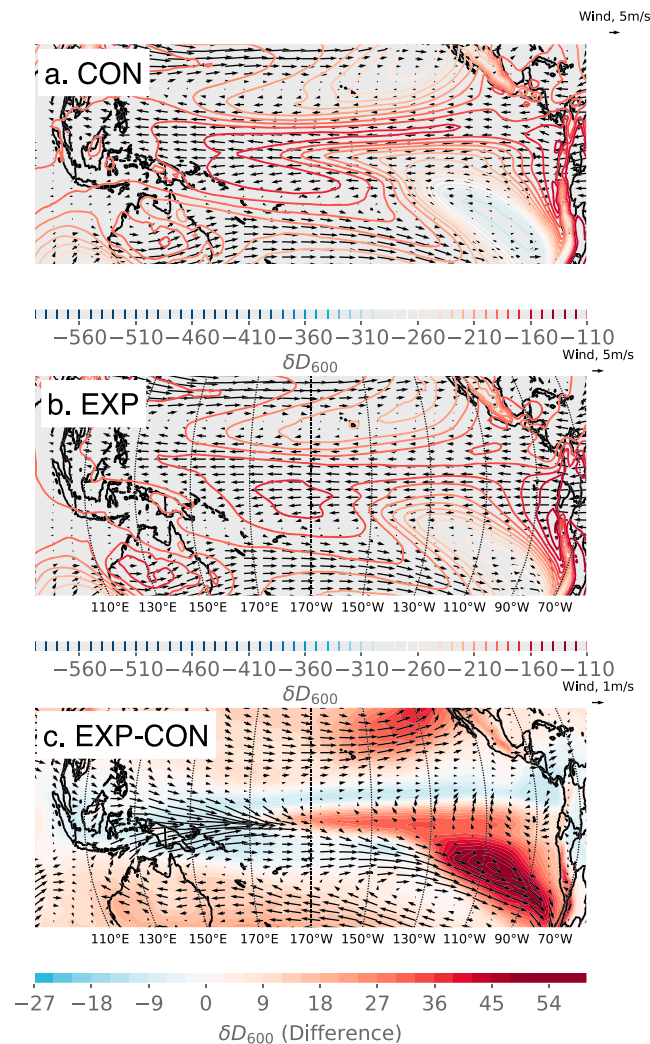
Figure 8. Changes in winds superposed on isotopes in water vapor, iCAM5. Changes in advection can be explained via changes in the winds and the spatial pattern of water isotopes in vapor at the 600-hPa level. Change in winds (vectors) and simulated isotope ratios in water vapor, (a) control, (b) experiment, and (c) experiment minus control.

3.3.5. Net Isotopic Response and Comparison to Satellite Observations

All of the above-mentioned circulation impacts to midtropospheric water vapor emerge in the west-east gradient in δD_V across the tropical Pacific (Figure 9). The figure shows a horizontal cross section through the 600 hPa for both ω (a) and δD_V (b) in the experiment versus control for iCAM5. Panel (a) shows changes in ω suggesting decreased upward motion in the western Pacific and decreased subsidence over the central and eastern Pacific, together indicating a slowing of the Walker circulation. Examining the δD_V (Figure 9c), the high-CO_2 experiment (red line) over the IPWP shows that δD_V is lower than the control experiment (blue line). In this region, increased moisture in the troposphere leads to more enriched δD_V. Convection enriches the midtroposphere, and less uplift/convection would decrease the HDO enrichment. In essence, decreased convection in the western Pacific leads to less water lofted into the midtroposphere, accompanied by a decrease in δD_V. Conversely, in the eastern Pacific, the δD_V values are more enriched due to increasing temperatures. Reduced subsidence would also allow convective mixing with moist boundary layer air to further enrich midtropospheric vapor and would lessen drying of midtropospheric air and mixing with HDO-depleted upper-tropospheric water masses. Together, these processes drive a robust isotopic signal of changes in tropical circulation.

In the high-CO_2 experiment, the west-east gradient in midtrophospheric δD_V over the tropical Pacific weakens (Figure 9c). If δD_V decreases with decreased convective uplift, higher E−P, and reduced advection of isotopi-
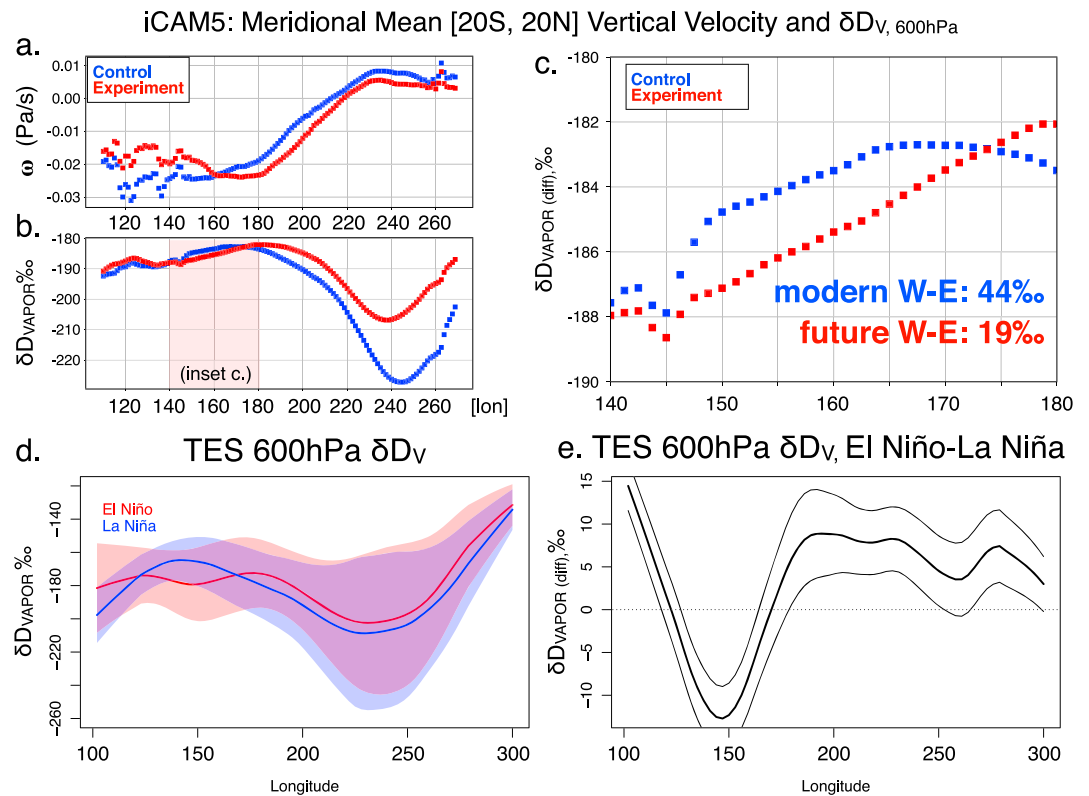
Figure 9. iCAM5 results: changes in vapor isotopes and ω across the tropical Pacific (W−E). (a) Future (warmer climate) and modern ω, (b) future (warmer climate) and modern δD_V at 500–600 hPa, and (c) inset for simulated changes in the western Pacific (145 to 180°E). Changes in δD vertical gradients may serve as a tracer for future changes to the tropical hydrological cycle. (d, e) Tropospheric Emission Spectrometer (TES) retrievals across the Walker cell: (d) Midtropospheric tropical δD_V estimated from TES satellite retrievals for El Niño and La Niña and (e) the mean difference between these weak and strong Walker circulation periods, respectively. Midtropospheric TES δD_V is calculated from joint retrievals of HDO and H_2O volume mixing ratios near the 620-hPa level, using the TES Lite version 6 data set (TES Science Team, 2013). The retrievals are filtered to ensure at least 0.5 degrees of freedom in the HDO vertical profile and a mean cloud optical depth less than 3.6. HDO and H_2O concentrations are then averaged daily to a $3 \times 3°$ grid before being averaged across weak and strong Walker circulation periods. El Niño-Southern Oscillation composites are defined by the months September–February with seasons 2006–2007 and 2009–2010 representing moderate El Niño conditions (weak Walker circulation) and seasons 2007–2008 and 2010–2011 representing moderate La Niña conditions (strong Walker circulation). Solid lines in panel (d) represent meridional means (spanning 21°S to 21°N) for each composite, with the shading representing the standard error around the meridional estimate ($n = 13$). The meridional means and their errors are smoothed using a span of 0.25. The thick black line in panel (e) represents the mean difference between El Niño and La Niña composites at each meridian, with the thin black lines representing the standard error of the mean difference estimate ($n = 13$). As in panel (d), the lines are smoothed using a span of 0.25.

cally enriched moisture in the western Pacific and simultaneously increase due to reduced subsidence and weakened easterlies in the eastern Pacific, the west minus east (W−E) *difference* in δD_V will decrease as a direct impact of circulation changes (Figure 9c). The W−E gradient in iCAM5 is 44‰ in the modern control and 19‰ in the high-CO_2 warmer climate, which in total shows a shallowing in the W−E gradient of ∼25‰ (a 56% reduction) with a doubling of CO_2. To quantify the extent to which the W−E gradient response in δD_V is dynamic versus thermodynamic, we computed the same gradient for the Rayleigh-predicted response in the single-column model for both regions. We obtain a difference of ∼7.5‰ due to temperature alone, indicating that approximately 70% of the response is due to changes in circulation. The total shift of 25‰ is sufficiently large to be detectable via remote sensing. We propose that W−E gradient in δD_V in the midtroposphere will be reduced with future warming and serves as a dynamical fingerprint of changes in the strength of the Walker circulation.

4. Discussion: Detecting Changes in the Walker Circulation

Global warming will have large impacts on the global hydrological cycle, but these impacts remain uncertain (Intergovernmental Panel on Climate Change, 2013). This work highlights the utility of water isotope ratios to detect large-scale changes in the hydrological cycle and the Walker circulation in a warmer world. Both GCM and Rayleigh single-column model results indicate that there is a dominant thermodynamic impact on isotope ratios at most heights in the atmosphere, as warming coupled with higher humidity tend to enrich isotopes in water vapor.

However, in high-CO_2 model simulations, isotope ratios in the midtroposphere ($\sim 700–500$ hPa) are depleted relative to expectations from thermodynamics alone. This isotopic depletion is driven by dynamical changes in the tropical Pacific, the impacts of which are quantifiable. Simulations show vertical velocity slowing (less upward motion in the west and less downward motion in the east). Consequently, isotope ratios decrease in the west and increase in the east, consistent with changes in vertical moisture transport. The resulting W−E δD_V gradient is reduced with a weakening Walker circulation, potentially providing a diagnostic for past and future changes in the overturning circulation. Dynamically-driven changes in water vapor isotopes are large enough to detect and provide targets for future satellite retrievals.

Further, spatial variations in isotope ratios in the tropical Pacific show sensitivity to variables beyond a simple W−E gradient in ω. Changes along the ITCZ and South Pacific convergence zone are consistent with increasing condensation (cloud content) and precipitation, while increasing δD_V along the eastern ITCZ and southeast tropical Pacific are likely dominated by slowing easterlies and changes in advection. Changes in isotope ratios provide much more than a record of changing vertical velocity: they are an indicator of the reorganization of tropical convection and its relationship to the large-scale Walker circulation.

Monitoring future changes would require a joint modeling and observational effort to track changes to the mean tropical circulation and, in particular, the strength of the Walker circulation in a warmer atmosphere using water isotopes. Water isotope monitoring and remote sensing campaigns are generally sparse in both space and time, especially for water vapor (e.g., Steen-Larsen et al., 2017). Such monitoring is critical for the validation of isotope-enabled climate models. Water vapor isotope ratios are now regularly measured by satellite missions, which measure upwelling radiance in different spectral bands sensitive to the absorption of water vapor. At present, available satellite products include total column (Scanning Imaging Absorption Spectrometer for Atmospheric Chartography, Frankenberg et al., 2009), midtropospheric (450 to 850 hPa, Tropospheric Emission Spectrometer, TES Field et al., 2014), multilevel measurements of water vapor at 100-hPa spacing, sensitive between 2- and 8-km altitude, from the Infrared Atmospheric Sounding Interferometer (Pougatchev et al., 2009; Schneider et al., 2015; Siméoni et al., 1997), and upper-tropospheric (Advanced Composition Explorer and Michelson Interferometer for Passive Atmospheric Sounding) HDO/H_2O (Bernath et al., 2005; Fischer et al., 2008). Satellite products for HDO often exhibit large differences and contain biases of up to 30‰ (Risi et al., 2012). TES does capture the impacts of rainout and the Walker circulation in the tropical Pacific, but measures a large range of altitudes.

What precision is needed in satellite data products to capture (1) a change in the W−E gradient in δD_V in the midtroposphere and thus (2) anthropogenic impacts on the hydrological cycle with water isotopes? Currently, available satellite missions measure δD_V in the atmospheric boundary layer, the free atmosphere, or total column; our study suggests that more accurate midtroposphere measurements (above ~ 700 hPa) may be needed to detect changes in convective mass flux using water vapor isotope ratios. Recent work using TES observations across El Niño-Southern Oscillation events show variations of 20–40‰ in δD_V suggesting that it is possible to distinguish between warmer and colder phases in the tropical Pacific and related circulation changes (Bailey et al., 2017). Figures 9d, 9e, and S6 show the difference in water isotopes in vapor in TES satellite retrievals for composite ENSO events spanning 2004–2011 and compares changes in ω to observations of water isotope ratios and iCAM5-simulated δD_V. These observations, though limited in time, suggest circulation changes with ENSO leave an isotopic fingerprint (Bailey et al., 2017) and that a decelerated Walker tends toward El Niño-like conditions (in agreement with Vecchi & Soden, 2007). Further, Figures 9d and 9e show that δD_V estimated from TES satellite retrievals for El Niño versus La Niña are consistent with the models' future prediction of a shoaling W−E gradient in δD_V with mean warming. Thus, we assert that there is large potential, with future improvements to these satellite retrievals of HDO and H_2O, to capture dynamical changes captured by water isotopes in midtroposphere. Even though ENSO is not an exact proxy for changes in the Walker circulation with global warming, the Walker circulation does weaken during El Niño compared

to La Niña (Vecchi & Soden, 2007). There is thus reason to believe that satellite retrievals of isotope ratios in water vapor are capable of detecting isotopic changes caused by a weakening of the Walker circulation.

This work also harbors important implications for paleoclimate interpretations of isotopic reconstructions in the tropics. Our analysis indicates that water isotopes are strongly affected by thermodynamic processes in the free troposphere, including in the tropics where the impacts of temperature on water isotope records are usually not considered. Rather, paleoclimate reconstructions from the deep tropics have primarily focused on the changes in the hydrological cycle and precipitation amount. Our analysis shows that the impacts of temperature on water isotope ratios should be fully considered in the climate reconstructions and via additional work with coupled GCMs. Further, rain primarily forms in the lower atmosphere (the boundary layer or lower-middle free troposphere) where moisture concentrations are higher, providing added evidence that proxies that record rain amount will capture a lower-atmospheric signal largely controlled by thermodynamics. Changes due to circulation or a reorganization of the hydrological cycle might prove difficult to tease apart from thermodynamic changes in geochemical archives of past climate. These complications highlight the importance of the use of water isotope-enabled models and proxy system models (e.g., Dee, Emile-Geay, et al., 2015) in paleoclimate data-model comparison.

We acknowledge important caveats to this study. The results presented here are specific to one isotope-enabled model, iCAM5. A comparison of observations (TES) and iCAM5 suggests that this model provides a realistic simulation of midtroposphere isotope ratios in the present (supporting information Figure S6 compares ERA-Interim reanalysis ω values and TES δD_V to community atmosphere model version 5 for ENSO event composites). Because of iCAM5's strong agreement with available observations, we assert that our methodology puts forth an important test for other models. A companion simulation with IsoGSM reveals that both models show changes in ω consistent with a slowing Walker cell in a warming atmosphere (Figures S3 and S4), weakening easterly winds aloft (Figure S10), and anomalous depletion of midtropospheric δD_V in the central tropical Pacific (Figure S5)—a result that provides confidence as it is common to both models. However, differences emerge between the two state-of-the-art GCMs, in part because the forcing and control simulations differ (see supporting information section S1.2). IsoGSM shows characteristic differences in its simulation of isotope ratios with height, which, coupled with differences among models in the advection term (Figure S9), results in large differences in water vapor isotope profiles and spatial patterns. IsoGSM's signal of isotopic depletion in the warming simulation is localized to the south central Pacific rather than the western Pacific as in iCAM5. Figures S3 and S4 show that the longitudinal changes in the strength of the Walker are also different in both models. We expect different circulation responses due to different forcing and also different isotope physics parameterizations.

To this end, differences in the simulation of midtropospheric isotope ratio profiles should be diagnosed across a suite of isotope-enabled models (e.g., Table S1 , Hoffman et al., 1998; Kurita et al., 2011; Liu et al., 2014; Mathieu et al., 2002; Mignot & Bony, 2013; Noone, 2002; Peixoto & Oort, 1992; Reuter et al., 2018; Risi et al., 2010; Schmidt et al., 2007; Tindall et al., 2009; Werner et al., 2011). Such simulations need to employ identical CO_2 and SST forcing in order to evaluate intermodel differences in the isotopic response. Comparison across multiple models is crucial for establishing robust isotope diagnostics of changes in the tropical overturning circulation. In future work, we hope to perform an isotope-enabled model intercomparison project investigating changes in the Walker cell as recorded by midtropospheric isotopes in vapor, focusing on differences in, for example, models' cloud physics. Such work is ongoing.

Better diagnostics are needed for the many processes impacting isotopes in vapor related to circulation (e.g., impacts of residence time, Aggarwal et al., 2012; divergence, Bailey et al., 2017; Lee et al., 2007; precipitation efficiency, Bailey et al., 2015; cloud physics, Moore et al., 2016; and updraft strength on the isotopic signal Bolot et al., 2013), and we have yet to fully address the impact of horizontal transport, potentially using water tracer/tagging experiments. Further, recent modeling work has challenged the relationship between global convective mass flux M and the strength of the Walker circulation, which is formally defined by SLP gradients in the tropical Pacific (Sandeep et al., 2014). The dynamical controls on changes in the Walker circulation require further observation and a greater diversity in model simulations. Finally, recent work demonstrating the utility of incorporating of water isotope ratios in data assimilation-based reanalyses may provide more advanced data products with which to investigate the relationships between M and δD_V (Yoshimura et al., 2014).

Changes to the dynamics of the hydrological cycle in response to global warming will be caused in part by increased atmospheric water vapor, which amplifies other climate system feedbacks (Schneider et al., 2010).

Further, uncertainties in the simulation of convective processes are currently a major source of uncertainty in projections of future climate and climate sensitivity estimates (e.g., Sherwood et al., 2014, 2015). Water isotopes in both GCMs and satellite-derived observations provide a quantitative measure changes in convective mass transport in the atmosphere and, more globally, help diagnose changes to the atmospheric water cycle on a warmer planet. This study lays the groundwork for large-scale detection of changes in the strength of the Walker circulation and trends in vertical mass transport observable in water isotope space. This is a first step in setting targets for remote sensing and in situ observations of future changes to the hydrological cycle.

References

Aggarwal, P. K., Alduchov, O. A., Froehlich, K. O., Araguas-Araguas, L. J., Sturchio, N. C., & Kurita, N. (2012). Stable isotopes in global precipitation: A unified interpretation based on atmospheric moisture residence time. *Geophysical Research Letters*, *39*, L11705. https://doi.org/10.1029/2012GL051937

An, S.-I., Kim, J.-W., Im, S.-H., Kim, B.-M., & Park, J.-H. (2012). Recent and future sea surface temperature trends in tropical Pacific warm pool and cold tongue regions. *Climate dynamics*, *39*(6), 1373–1383.

Bailey, A., Blossey, P., Noone, D., Nusbaumer, J., & Wood, R. (2017). Detecting shifts in tropical moisture imbalances with satellite-derived isotope ratios in water vapor. *Journal of Geophysical Research: Atmospheres*, *122*, 5763–5779. https://doi.org/10.1002/2016JD026222

Bailey, A., Nusbaumer, J., & Noone, D. (2015). Precipitation efficiency derived from isotope ratios in water vapor distinguishes dynamical and microphysical influences on subtropical atmospheric constituents. *Journal of Geophysical Research: Atmospheres*, *120*, 9119–9137. https://doi.org/10.1002/2015JD023403

Bernath, P. F., McElroy, C. T., Abrams, M. C., Boone, C. D., Butler, M., Camy-Peyret, C., et al. (2005). Atmospheric Chemistry Experiment (ACE): Mission overview. *Geophysical Research Letters*, *32*, L15S01. https://doi.org/10.1029/2005GL022386

Betts, A. K. (1998). Climate-convection feedbacks: Some further issues. *Climatic Change*, *1*(39), 35–38.

Bolot, M., Legras, B., & Moyer, E. (2013). Modelling and interpreting the isotopic composition of water vapour in convective updrafts. *Atmospheric Chemistry and Physics*, *13*(16), 7903–7935.

Carilli, J. E., McGregor, H. V., Gaudry, J. J., Donner, S. D., Gagan, M. K., Stevenson, S., et al. (2014). Equatorial Pacific coral geochemical records show recent weakening of the Walker circulation. *Paleoceanography*, *29*, 1031–1045. https://doi.org/10.1002/2014PA002683

Conroy, J. L., Restrepo, A., Overpeck, J. T., Steinitz-Kannan, M., Cole, J. E., Bush, M. B., & Colinvaux, P. A. (2009). Unprecedented recent warming of surface temperatures in the eastern tropical Pacific Ocean. *Nature geoscience*, *2*(1), 46–50.

Dee, S., Emile-Geay, J., Evans, M., Allam, A., Steig, E., & Thompson, D. (2015). PRYSM: An open-source framework for proxy system modeling, with applications to oxygen-isotope systems. *Journal of Advances in Modeling Earth Systems*, *7*, 1220–1247. https://doi.org/10.1002/2015MS000447

Dee, S., Noone, D., Buenning, N., Emile-Geay, J., & Zhou, Y. (2015). SPEEDY-IER: A fast atmospheric GCM with water isotope physics. *Journal of Geophysical Research: Atmospheres*, *120*, 73–91. https://doi.org/10.1002/2014JD022194

DiNezio, P., Clement, A., Vecchi, G., Soden, B., Broccoli, A., Otto-Bliesner, B., & Braconnot, P. (2011). The response of the Walker circulation to Last Glacial Maximum forcing: Implications for detection in proxies. *Paleoceanography*, *26*, PA3217. https://doi.org/10.1029/2010PA002083

DiNezio, P. N., Clement, A. C., Vecchi, G. A., Soden, B. J., Kirtman, B. P., & Lee, S.-K. (2009). Climate response of the equatorial Pacific to global warming. *Journal of Climate*, *22*(18), 4873–4892.

Field, R. D., Kim, D., LeGrande, A. N., Worden, J., Kelley, M., & Schmidt, G. A. (2014). Evaluating climate model performance in the tropics with retrievals of water isotopic composition from Aura TES. *Geophysical Research Letters*, *41*, 6030–6036. https://doi.org/10.1002/2014GL060572

Fischer, H., Birk, M., Blom, C., Carli, B., Carlotti, M., von Clarmann, T., et al. (2008). MIPAS: An instrument for atmospheric and climate research. *Atmospheric Chemistry and Physics*, *8*(8), 2151–2188.

Frankenberg, C., Yoshimura, K., Warneke, T., Aben, I., Butz, A., Deutscher, N., et al. (2009). Dynamic processes governing lower-tropospheric HDO/H_2O ratios as observed from space and ground. *Science*, *325*(5946), 1374–1377. https://doi.org/10.1126/science.1173791

Galewsky, J., Steen-Larsen, H. C., Field, R. D., Worden, J., Risi, C., & Schneider, M. (2016). Stable isotopes in atmospheric water vapor and applications to the hydrologic cycle. *Reviews of Geophysics*, *54*, 809–865. https://doi.org/10.1002/2015RG000512

Gastineau, G., Li, L., & Le Treut, H. (2009). The Hadley and Walker circulation changes in global warming conditions described by idealized atmospheric simulations. *Journal of Climate*, *22*(14), 3993–4013.

Held, I. M., & Soden, B. J. (2006). Robust responses of the hydrological cycle to global warming. *Journal of Climate*, *19*, 5686–5699. https://doi.org/10.1175/JCLI3990.1

Hoffmann, G., Werner, M., & Heimann, M. (1998). Water isotope module of the ECHAM atmospheric general circulation model: A study on timescales from days to several years. *Journal of Geophysical Research*, *103*(NO. D14), 16,871–16,896.

Huntington, T. G. (2006). Evidence for intensification of the global water cycle: Review and synthesis. *Journal of Hydrology*, *319*(1), 83–95.

Hurrell, J. W., Holland, M. M., Gent, P. R., Ghan, S., Kay, J. E., Kushner, P. J., et al. (2013). The Community Earth System Model: A framework for collaborative research. *Bulletin of the American Meteorological Society*, *94*(9), 1339–1360. https://doi.org/10.1175/BAMS-D-12-00121.1

Intergovernmental Panel on Climate Change (2013). *Summary for policymakers* (pp. 1–30), book section SPM. Cambridge United Kingdom and New York, NY, USA: Cambridge University Press. https://doi.org/10.1017/CBO9781107415324.004

Jenkins, H. (2008). Clausius-Clapeyron Equation. *Chemical Thermodynamics at a Glance* (pp. 76–77).

Kurita, N., Noone, D., Risi, C., Schmidt, G. A., Yamada, H., & Yoneyama, K. (2011). Intraseasonal isotopic variation associated with the Madden-Julian Oscillation. *Journal of Geophysical Research (1984–2012)*, *116*, D24101. https://doi.org/10.1029/2010JD015209

LHeureux, M. L., Lee, S., & Lyon, B. (2013). Recent multidecadal strengthening of the Walker circulation across the tropical Pacific. *Nature Climate Change*, *3*(6), 571–576.

Lee, J.-E., Fung, I., DePaolo, D. J., & Henning, C. C. (2007). Analysis of the global distribution of water isotopes using the NCAR atmospheric general circulation model. *Journal of Geophysical Research*, *112*, D16306. https://doi.org/10.1029/2006JD007657

Liu, Z., Yoshimura, K., Bowen, G. J., Buenning, N. H., Risi, C., Welker, J. M., & Yuan, F. (2014). Paired oxygen isotope records reveal modern North American atmospheric dynamics during the holocene. copyright - Copyright Nature Publishing Group Apr 2014; Last updated - 2014-05-06.

Loaiciga, H. A., Valdes, J. B., Vogel, R., Garvey, J., & Schwarz, H. (1996). Global warming and the hydrologic cycle. *Journal of Hydrology*, *174*(1-2), 83–127.

Majoube, M. (1971). Fractionement en oxygene 18 et en deuterium entre l'eau et sa vapeur. *Journal de Chimie Physique et de Physico-Chimie Biologique*, *68*, 625–636. 1423–1436.

Mapes, B. E. (2001). Water's two height scales: The moist adiabat and the radiative troposphere. *Quarterly Journal of the Royal Meteorological Society*, *127*(577), 2353–2366.

Mathieu, R., Pollard, D., Cole, J. E., White, J. W., Webb, R. S., & Thompson, S. L. (2002). Simulation of stable water isotope variations by the GENESIS GCM for modern conditions. *Journal of Geophysical Research*, *107*(D4), 4037. https://doi.org/10.1029/2001JD900255

Mignot, J., & Bony, S. (2013). Presentation and analysis of the IPSL and CNRM climate models used in CMIP5. *Climate Dynamics*, *40*(2089), 2089.

Moore, M., Blossey, P., Muhlbauer, A., & Kuang, Z. (2016). Microphysical controls on the isotopic composition of wintertime orographic precipitation. *Journal of Geophysical Research: Atmospheres*, *121*, 7235–7253. https://doi.org/10.1002/2015JD023763

Moore, M., Kuang, Z., & Blossey, P. (2014). A moisture budget perspective of the amount effect. *Geophysical Research Letters*, *41*(4), 1329–1335.

Noone, D. (2002). Annular variations in moisture transport mechanisms and the abundance of δ^{18}O in Antarctic snow. *Journal of Geophysical Research*, *107*(D24), 4742. https://doi.org/10.1029/2002JD002262

Noone, D. (2012). Pairing measurements of the water vapor isotope ratio with humidity to deduce atmospheric moistening and dehydration in the tropical midtroposphere. *Journal of Climate*, *25*(13), 4476–4494.

Nusbaumer, J., Wong, T. E., Bardeen, C., & Noone, D. (2017). Evaluating hydrological processes in the Community Atmosphere Model version 5 (CAM5) using stable isotope ratios of water. https://doi.org/10.1002/2016MS000839

Park, S., Bretherton, C. S., & Rasch, P. J. (2014). Integrating cloud processes in the Community Atmosphere Model, version 5. *Journal of Climate*, *27*(18), 6821–6856.

Peixoto, J. P., & Oort, A. H. (1992). *Physics of climate* (pp. 520). Melville, New York: AIP-Press.

Pougatchev, N., August, T., Calbet, X., Hultberg, T., Oduleye, O., Schlüssel, P., et al. (2009). IASI temperature and water vapor retrievals—Error assessment and validation. *Atmospheric Chemistry and Physics*, *9*(17), 6453–6458.

Reuter, J., Buenning, N., & Yoshimura, K. (2018). Evaluating hydrological influences on mid-latitude δ18Op in the Middle East. *Climate Dynamics*, *50*(9-10), 3153–3170.

Riahi, K., Rao, S., Krey, V., Cho, C., Chirkov, V., Fischer, G., et al. (2011). RCP 8.5—A scenario of comparatively high greenhouse gas emissions. *Climatic Change*, *109*(1-2), 33–57.

Risi, C., Bony, S., Vimeux, F., & Jouzel, J. (2010). Water-stable isotopes in the LMDZ4 general circulation model: Model evaluation for present-day and past climates and applications to climatic interpretations of tropical isotopic records. *Journal of Geophysical Research (1984–2012)*, *115*, D12118. https://doi.org/10.1029/2009JD013255

Risi, C., Noone, D., Worden, J., Frankenberg, C., Stiller, G., Kiefer, M., et al. (2012). Process-evaluation of tropospheric humidity simulated by general circulation models using water vapor isotopologues: 1. Comparison between models and observations. *Journal of Geophysical Research*, *117*, D05303. https://doi.org/10.1029/2011JD016621

Sandeep, S., Stordal, F., Sardeshmukh, P. D., & Compo, G. P. (2014). Pacific Walker circulation variability in coupled and uncoupled climate models. *Climate dynamics*, *43*(1-2), 103–117.

Schmidt, G. A., LeGrande, A. N., & Hoffmann, G. (2007). Water isotope expressions of intrinsic and forced variability in a coupled ocean-atmosphere model. *Journal of Geophysical Research (1984–2012)*, *112*, D10103. https://doi.org/10.1029/2006JD007781

Schneider, M., González, Y., Dyroff, C., Christner, E., Wiegele, A., Barthlott, S., et al. (2015). Empirical validation and proof of added value of MUSICA's tropospheric δd remote sensing products. *Atmospheric Measurement Techniques Discussions*, *7*, 6917–6969.

Schneider, T., O'Gorman, P. A., & Levine, X. J. (2010). Water vapor and the dynamics of climate changes. *Reviews of Geophysics*, *48*, RG3001. https://doi.org/10.1029/2009RG000302

Seager, R., Naik, N., & Vecchi, G. A. (2010). Thermodynamic and dynamic mechanisms for large-scale changes in the hydrological cycle in response to global warming. *Journal of Climate*, *23*(17), 4651–4668.

Sharp, Z. (2007). *Principles of stable isotope geochemistry*. Upper Saddle River, NJ: Pearson Prentice Hall.

Sherwood, S. C., Bony, S., & Dufresne, J.-L. (2014). Spread in model climate sensitivity traced to atmospheric convective mixing. *Nature*, *505*(7481), 37–42.

Sherwood, S., Webb, M., Lock, A., Bretherton, C. S., Bony, S., Cole, J. N., et al. (2015). Do convective schemes substantially alter simulated global climate and cloud feedback? In *AGU Fall Meeting Abstracts*, pp. A33R–03.

Siméoni, D., Singer, C., & Chalon, G. (1997). Infrared atmospheric sounding interferometer. *Acta Astronautica*, *40*(2-8), 113–118.

Soden, B. J., & Held, I. M. (2006). An assessment of climate feedbacks in coupled ocean–atmosphere models. *Journal of Climate*, *19*(14), 3354–3360.

Sohn, B., & Park, S.-C. (2010). Strengthened tropical circulations in past three decades inferred from water vapor transport. *Journal of Geophysical Research*, *115*, D15112. https://doi.org/10.1029/2009JD013713

Steen-Larsen, H., Risi, C., Werner, M., Yoshimura, K., & Masson-Delmotte, V. (2017). Evaluating the skills of isotope-enabled general circulation models against in situ atmospheric water vapor isotope observations. *Journal of Geophysical Research: Atmospheres*, *122*, 246–263. https://doi.org/10.1002/2016JD025443

TES Science Team, N. A. S. D. C. A. (2013). TES/Aura level 2, HDO Limb, version 6, Hampton, VA, USA: Accessed TES/Aura L2 Deuterium Oxide (HDO) Lite Nadir (TL2HDOLN). https://doi.org/10.5067/AURA/TES/TL2HDOLN_L2.006

Tindall, J. C., Valdes, P. J., & Sime, L. C. (2009). Stable water isotopes in HadCM3: Isotopic signature of El Niño Southern Oscillation and the tropical amount effect. *Journal of Geophysical Research*, *114*, D04111. https://doi.org/10.1029/2008JD010825

Tokinaga, H., Xie, S.-P., Timmermann, A., McGregor, S., Ogata, T., Kubota, H., & Okumura, Y. M. (2012). Regional patterns of tropical Indo-Pacific climate change: Evidence of the Walker circulation weakening. *Journal of Climate*, *25*(5), 1689–1710.

Torri, G., Ma, D., & Kuang, Z. (2017). Stable water isotopes and large-scale vertical motions in the tropics. *Journal of Geophysical Research: Atmospheres*, *122*, 3703–3717. https://doi.org/10.1002/2016JD026154

Vecchi, G., Clement, A., & Soden, B. (2008). Examining the tropical Pacific's response to global warming. *Eos Transactions American Geophysical Union*, *89*(9), 81–83.

Vecchi, G. A., & Soden, B. J. (2007). Global warming and the weakening of the tropical circulation. *Journal of Climate*, *20*(17), 4316–4340.

Vecchi, G. A., Soden, B. J., Wittenberg, A. T., Held, I. M., Leetmaa, A., & Harrison, M. J. (2006). Weakening of tropical Pacific atmospheric circulation due to anthropogenic forcing. *Nature*, *441*, 73–76.

Wallace, J. M., & Hobbs, P. V. (2006). *Atmospheric science: An introductory survey*, vol. 92. Cambridge, Massachusetts, United States: Academic press.

Wentz, F. J., Ricciardulli, L., Hilburn, K., & Mears, C. (2007). How much more rain will global warming bring? *Science*, *317*(5835), 233–235.

Werner, M., Langebroek, P. M., Carlsen, T., Herold, M., & Lohmann, G. (2011). Stable water isotopes in the ECHAM5 general circulation model: Toward high-resolution isotope modeling on a global scale. *Journal of Geophysical Research*, *116*, D15109. https://doi.org/10.1029/2011JD015681

Wong, T. E., Nusbaumer, J., & Noone, D. C. (2017). Evaluation of modeled land-atmosphere exchanges with a comprehensive water isotope fractionation scheme in version 4 of the community land model. https://doi.org/10.1002/2016MS000842

Yoshimura, K., Kanamitsu, M., Noone, D., & Oki, T. (2008). Historical isotope simulation using reanalysis atmospheric data. *Journal of Geophysical Research*, *113*, D19108. https://doi.org/10.1029/2008JD010074

Yoshimura, K., Miyoshi, T., & Kanamitsu, M. (2014). Observation system simulation experiments using water vapor isotope information. *Journal of Geophysical Research: Atmospheres*, *119*, 7842–7862. https://doi.org/10.1002/2014JD021662